ISTITUTO NAZIONALE DI FISICA NUCLEARE
Laboratori Nazionali di Frascati

LNF-83/45

E. Burattini et al. : EXPERIMENTAL ACTIVITY AT THE ADONE WIGGLER FACILITY

Estratto da:
Nuclear Instr. and Meth. 208, 91 (1983)

Servizio Documentazione
dei Laboratori Nazionali di Frascati
Cas. Postale 13 - Frascati (Roma)

Nuclear Instruments and Methods 208 (1983) 91–96
North-Holland Publishing Company

EXPERIMENTAL ACTIVITY AT THE ADONE WIGGLER FACILITY

E. BURATTINI and A. REALE *
Istituto Nazionale di Fisica Nucleare, Laboratori Nazionali di Frascati, and CNR, Rome, Italy

E. BERNIERI, N. CAVALLO, A. MORONE, M.R. MASULLO and R. RINZIVILLO
Istituto Nazionale di Fisica Nucleare, Sezione di Napoli, and Istituto di Fisica Sperimentale dell'Università, Napoli, Italy

G. DALBA and P. FORNASINI
Dipartimento di Fisica dell'Università, Trento, Italy

C. MENCUCCINI
Istituto di Fisica della Facoltà di Ingegneria dell'Università, Rome, Italy

A short summary of the wiggler magnet beam lines and relative instrumentation installed at the Adone storage ring in Frascati is given. The future development of the wiggler laboratory is described. Preliminary results on the scientific activity in progress are presented.

1. Introduction

A conventional transverse wiggler magnet was installed into a straight section of the Adone storage ring in Frascati during 1980 to enhance the critical energy and to obtain a photon flux higher than the one emitted from a bending section. A first experimental station was also equipped inside the Adone hall and made available for preliminary work [1].

A new laboratory, outside the Adone building, about 30 m from the wiggler magnet, is presently being completed. In this laboratory the radiation emerging at small angles from the wiggler axis will be utilized as a second X-ray beam.

In this paper a brief description of the characteristics of the X-ray beam produced by the Adone wiggler magnet is given. The beam line, the monochromator and the data acquisition system are also described. In the last two sections of the paper some preliminary absorption spectroscopy results on the activity in progress and the future prospects are presented.

2. Experimental layout

In fig. 1 a schematic view of the Adone wiggler layout is given. The radiation emitted from the six full-poles equivalent magnet is travelling through a 12 m beam line, BX_1, including the monochromator and the sample chamber. The X-ray beam is presently utilized at an experimental station inside the machine hall. Such an arrangement implies some space limitations for the experimental apparatus and special personnel protection requirements. For these reasons all the apparatus is remotely controlled.

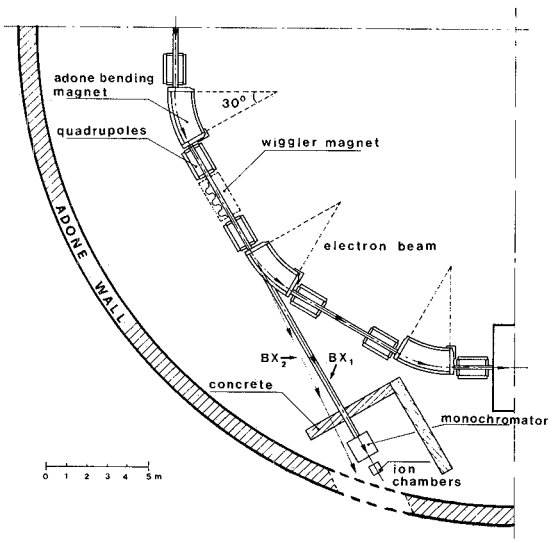

Fig. 1. Schematic view of the Adone wiggler layout in the present configuration.

* Now at the Università de'L'Aquila, Italy.

0167-5087/83/0000–0000/$03.00

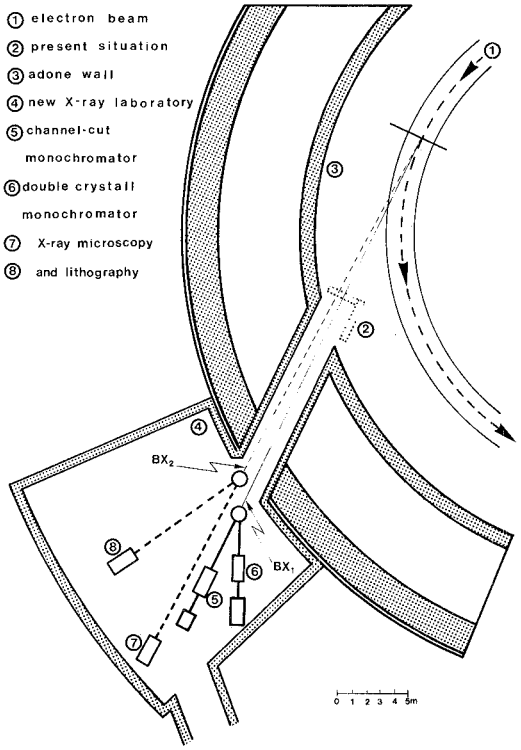

Fig. 2. Sketch of the new X-ray laboratory in the final configuration.

When the new dedicated experimental building will be completed (at the end of this year), the final configuration of the X-ray beam-lines will be like the one shown in fig. 2. The present BX_1 line will be split into two arms mainly dedicated to absorption and fluorescence spectroscopy, while the BX_2 line will be dedicated to X-ray microscopy and lithography.

The channel-cut monochromator will be transferred from the bunker inside the Adone hall to the new X-ray laboratory, while a double crystal monochromator, at present completely designed, will be built in the second part of the next year.

Table 1
Wiggler magnet characteristics.

Magnet period	654 mm
Number of poles	5 full + 2 half
Total length	2100 mm
Gap height	40 mm
Pole length at the gap	196 mm
Pole height	100 mm
Pole width at the gap	280 mm
Maximum field on axis	1.85 T
Excitation turns per pole	7
Copper weight	270 kg
Current	4500 A
Current density	18 A/mm^2
Total power	230 kW

3. Wiggler magnet

A conventional transverse wiggler magnet was built according to the characteristics listed in table 1.

The magnet length was chosen in order to fit the Adone straight section (2.50 m). The design specifications in terms of the field integral, at all fields, and the average multipole field coefficients in the transverse plane were met when proper correcting coils were used. The effects of the wiggler field on the optical parameters of the accelerator have been measured and found acceptable for the machine performance.

Maps of B_z on the magnet midplane were made for various supply currents: the relative accuracy in field values was better than 0.1% for $B > 1$ T and 0.05% for $B \leqslant 1$ T.

4. The beam line BX_1

The detailed scheme of the overall BX_1 beam line is sketched in fig. 3. The vacuum protection system is based on a fast valve (14 ms closing time) installed at the beginning of the pipe and on two electropneumatic valves. Alumina Cr-doped targets are used as synchro-

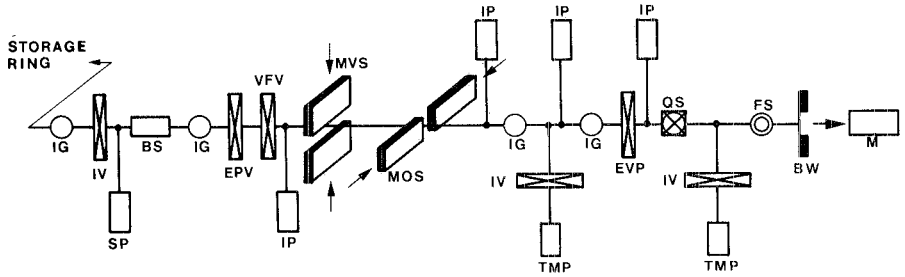

Fig. 3. Scheme of the BX_1 beam line: IG = ionization gauge; IV = isolation valve; SP = sublimation pump; BS = beam stopper; EVP = electropneumatic valve; VFV = very fast valve; IP = ionization pump; MVS(MOS) = motorized vertical (horizontal) slits; TMP = turbo-molecular pump; QS = quadrupole spectrometer; FS = fast sensor; BW = beryllium window; M = monochromator.

tron light monitors in two different points of the line. The pipe, which is equipped with a very fast copper beam stopper (50 ms closing time), presently terminates with a 144 μm thick beryllium window, 10 mm high and 20 mm wide. Several tests showed that the breaking of the beryllium window caused a pressure rise of about 10^{-9} Torr in the storage ring.

The distance from the center of the wiggler to the Be window is 13 m; consequently the horizontal angular acceptance of the beam line output is 1.5 mrad and the vertical angular acceptance is 0.8 mrad.

5. Beam characteristics

The spectral distribution of the radiation emerging from a single pole of the wiggler is shown in fig. 4 (full line); the one emitted from a bending magnet section of Adone is also reported (dotted line).

As expected, a comparison between the two distributions shows that the critical energy ϵ_c of the wiggler is higher by the ratio of the wiggler magnetic field B_w to the bending magnetic field B: in our case $B_w/B = 1.85$.

In table 2 the most important characteristics of the wiggler radiation are listed.

The dashed line in fig. 4 shows the spectral distribution after the Be window. The total power transmitted by the Be window has been computed to be 78 mW/mA in good agreement with the experimental value of 77 mW/mA measured by a calorimetric method.

Table 2
Wiggler radiation characteristics.

Total radiated power	13 W/mA
Critical energy	2.77 keV
Photon flux at $\lambda = \lambda_c$ (0.1% bw, $E = 1.5$ GeV, single pole)	2×10^{10} ph/s·mA·mrad
Horizontal angular acceptance at Be window	1.5 mrad
Vertical angular acceptance at Be window	0.8 mrad
Electron beam size	$\sigma_x = 1.8$ mm; $\sigma_z = 0.6$ mm
Maximum orbit displacement	10 mm

6. The experimental apparatus

An X-ray channel-cut monochromator has been designed, built, tested and operated in the beam line BX_1. The channel width of the two crystals used [Si(111) and Ge(220)] is 5 mm and the energy interval, in which the monochromator provides a very good photon flux, ranges from 3 keV to 31 keV; consequently the vertical displacement of the monochromatized beam is reduced to 2mm over the full energy range scanned.

Fig. 5 is an internal view of the instrument: the crystal mounting is connected to a Microcontrole rotating table, allowing rotations in steps of 10^{-3} degrees; two sets of remotely controlled micrometric tungsten

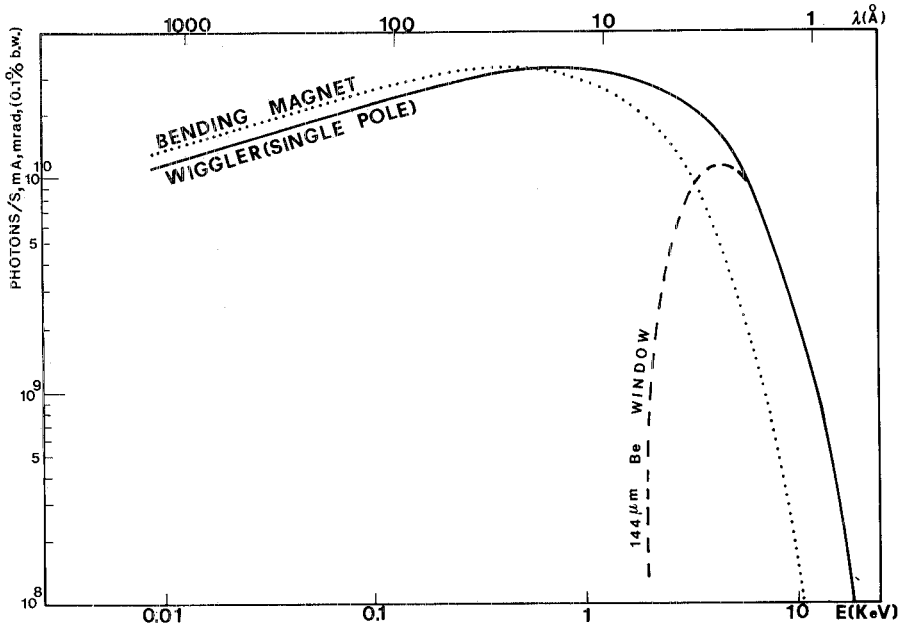

Fig. 4. Spectral distribution. Dotted line: Adone bending magnet; full line: Adone wiggler; dashed line: emerging from the Be window.

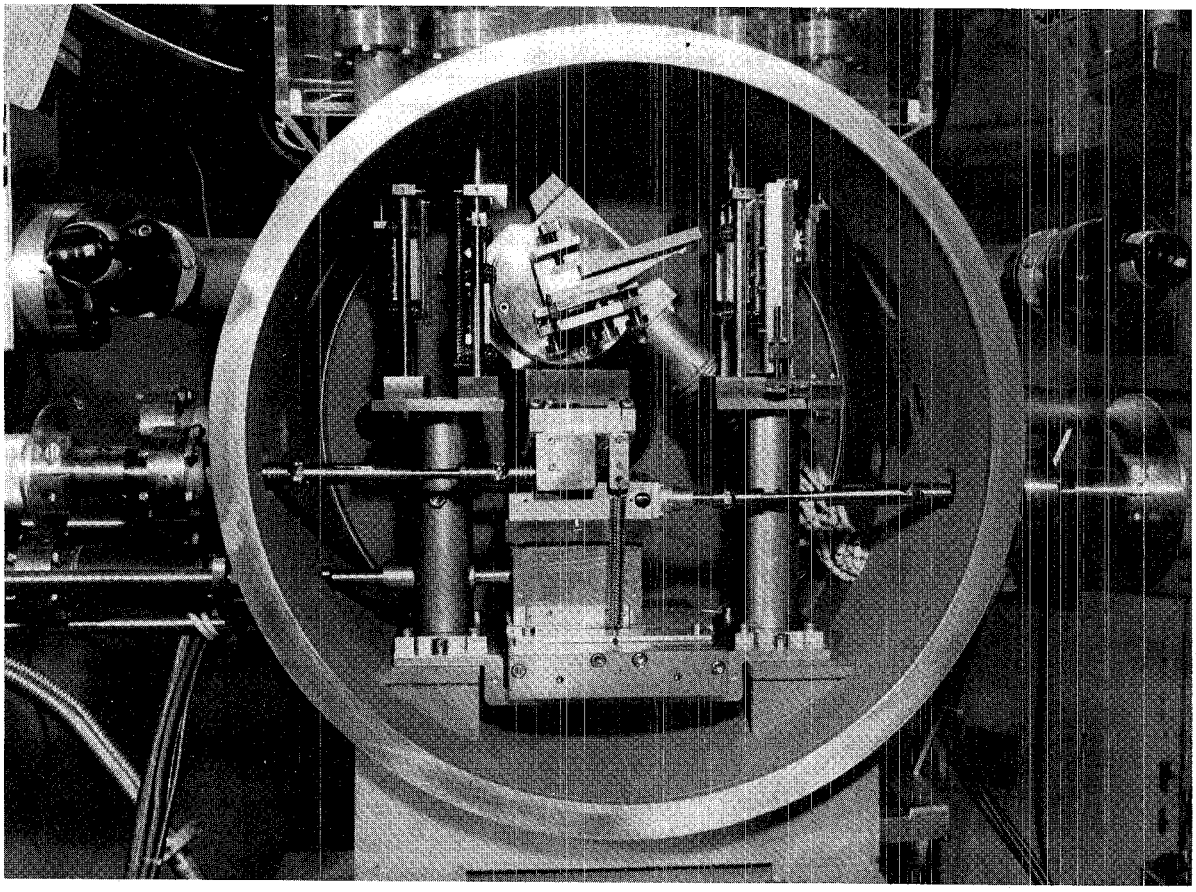

Fig. 5. Internal view of the monochromator showing the crystal mounting and the micrometric movements.

slits collimate the beam, and reduce the background radiation; several manual movements allow to adjust, very easily, the crystal orientation also when the monochromator is under vacuum conditions (about 10^{-8} Torr).

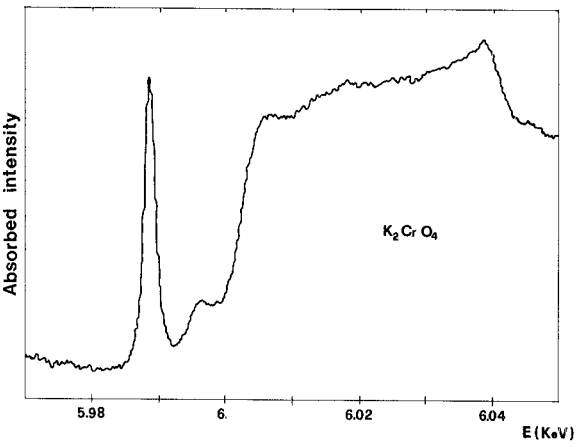

Fig. 6. K absorption edge of chromium in K_2CrO_4.

The chromium K absorption edge in K_2CrO_4, shown in fig. 6, exhibits a typical white peak with a fwhm of about 2 eV.Taking into account that the K-level width of chromium is estimated to be about 1 eV [2], one can conclude that in our experimental conditions the energy resolution of the monochromator is mainly determined by the intrinsic resolution of the crystal used [Si(111)] which can be calculated to be roughly 1 eV.

The detection system for absorption measurements consists of ionization chambers with plane-parallel electrodes. The cross-section of the active volume is 30×30 mm^2. Their windows are made of 20 μm thick Kapton. The chambers are normally operated with Ar or Kr and the gas pressure can be varied by remote control in the range 1–800 Torr.

Data collection and analysis are performed by a PDP 11/40 computer.

7. Experimental activity

The experiments up to now proposed or in progress at the wiggler facility concern absorption spectroscopy

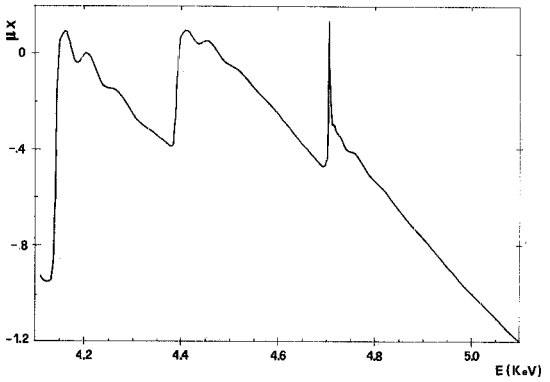

Fig. 7. L_{III}, L_{II}, L_{I} absorption edges of antimony in Sb_2S_5.

measurements (XANES and EXAFS) in solid state physics and biophysics.

7.1. Solid states physics program

(1) Paraelectric–ferroelectric phase transition in SbSI single crystals [3]. Fig. 7 shows the family of L edges of Sb in Sb_2S_5, a compound to be considered, together with Sb_2S_3 and SbI_3, as a standard for the interpretation of SbSI samples.

(2) Structure of superionic glasses containing AgI at various concentrations [4]. In fig. 8 the L_{III} absorption edge of Ag in $(AgI)_x$ $(Ag_2O_nB_2O_3)_{1-x}$ is reported. One can easily observe that different concentrations of AgI affect the site around the Ag atom.

(3) Characterization of the catalytic site in polystyrene–ruthenium catalyst. Some results on this subject have already been published [5].

Work soon to be done will include:

(i) Granular metallic compounds in order to analyze the alloy formation at low temperatures [6].

(ii) Temperature effects on the structure of amorphous and partially disordered semiconductors [7].

It is interesting to look at a typical high energy spectrum, say the K-edge of metallic cadmium (26.7

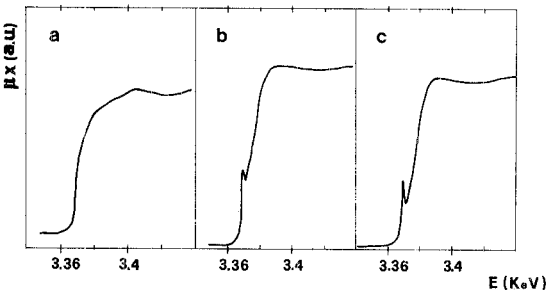

Fig. 8. L_{III} absorption edge of silver in: (a) crystalline AgI; (b) amorphous $(AgI)_{0.3}(Ag_2O_3\ 4\ B_2O)_{0.7}$; (c) amorphous $Ag_2O_3 4\ B_2O$.

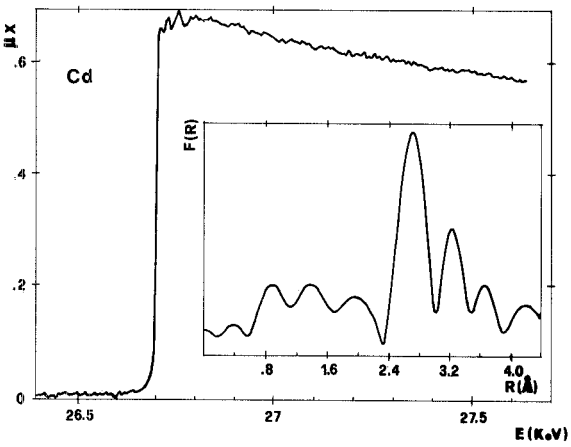

Fig. 9. EXAFS structures at the K absorption edge of metallic cadmium. The insert shows the amplitude of the Fourier transform.

keV) (fig. 9). The EXAFS oscillations, in this energy region, are smeared out, as is well known [8]. However one can still appreciate from the Fourier transform that the difference between the position of the main peak and the crystallographic distance of the nearest neighbours is in satisfactory agreement with the expected theoretical value [9].

7.2. Biophysics program

In biophysics our program concerns the study of the binding site of metallic ions, such as Mn^{2+}, Zn^{2+}, Cu^{2+}, etc., in biological macromolecules such as metalloproteins, nucleotides and nucleic acids [10].

In fig. 10 is reported the Fe K-edge in carp NO-hemoglobin and in metallic iron as a preliminary result on the conformational changes induced in the protein by

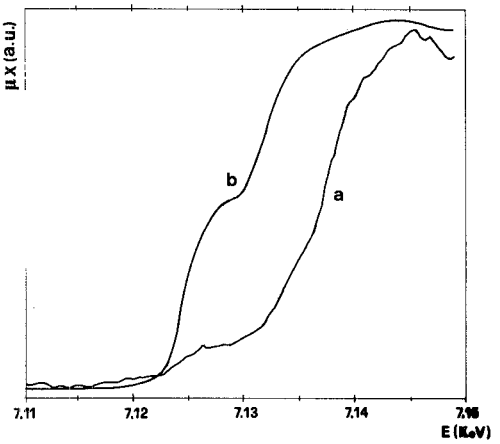

Fig. 10. K. absorption edge of Fe in: (a) carp NO-hemoglobin (20 mmol concentration); (b) metallic iron.

the presence of allosteric effectors like IHP (inositol-hexaphosphate) [11].

8. Conclusions

In the previous sections (1–6) the actual configuration of the beam line and the expected developments for the end of this year have been presented.

In section 7 the scientific activity was summarized.

The BX_1 line is meant to be used also in the future mainly for EXAFS and XANES measurements. In this context our programs involve, as an immediate step, the realization of a system of counters for fluorescence spectroscopy for samples with very small concentrations of absorbing atoms.

We also plan to develop a time-resolved X-ray spectroscopy apparatus. The second line BX_2 will be devoted to X-ray microscopy and lithography.

References

[1] R. Barbini et al., Riv. Nuovo Cim. 4 (1981).
[2] L.G. Parrat, Rev. Mod. Phys. 31 (1959) 616.
[3] In collaboration with the Azerbajan State University (USSR) and Istituto Superiore di Sanità, Rome, Italy.
[4] In collaboration with the Solid State Physics Group of the Physics Department, University of Trento, Italy.
[5] A. Bianconi et al., Chem. Phys. Lett. in press.
[6] In collaboration with a Solid State Group of the University of L'Aquila, Italy.
[7] In collaboration with the University of Parma, Italy.
[8] P. Rabe, G. Tolkiehn, A. Werner and R. Haensel, Z. Naturforsch. 34A (1979) 1528.
[9] B. Teo and P.A. Lee, J. Am. Chem. Soc. 101 (1979) 2815.
[10] In collaboration with the University of Rome and Istituto Superiore di Sanità, Rome, Italy.
[11] In collaboration with the University of Trento and the University of New York.